

Imaging through Scattering Media with a Learning Based Prior

Florian Schiffers¹, Lionel Fiske¹, Pablo Ruiz², Aggelos K. Katsaggelos², Oliver Cossairt^{1,2}

¹Computer Science, Northwestern University, Chicago, IL, USA

²Electrical and Computer Engineering, Northwestern University, Chicago, IL, USA

Abstract

Imaging through scattering media finds applications in diverse fields from biomedicine to autonomous driving. However, interpreting the resulting images is difficult due to blur caused by the scattering of photons within the medium. Transient information, captured with fast temporal sensors, can be used to significantly improve the quality of images acquired in scattering conditions. Photon scattering, within a highly scattering media, is well modeled by the diffusion approximation of the Radiative Transport Equation (RTE). Its solution is easily derived which can be interpreted as a Spatio-Temporal Point Spread Function (ST-PSF). In this paper, we first discuss the properties of the ST-PSF and subsequently use this knowledge to simulate transient imaging through highly scattering media. We then propose a framework to invert the forward model, which assumes Poisson noise, to recover a noise-free, unblurred image by solving an optimization problem.

Introduction

In recent years computational imaging has made significant advances due to both the advent new technologies, such as ultra fast cameras, and the increasing availability of computing resources. One area of interest is imaging through scattering media due to its applications to a myriad of fields such as biomedical imaging [1] or autonomous driving [2].

When light propagates through media such as fog or tissue it undergoes many scattering events causing a significant blur. A straightforward approach to imaging through scattering media is to image only the ballistic, i.e. non-scattered photons. Since these effects happen on very small time scales, direct measurement requires time-gating techniques with ultra-small acquisition times [3, 4]. However, relatively few ballistic photons reach the camera and time-gated images are dominated by Poisson noise. This problem can be circumvented by using time gating to separate photons which have been scattered progressively in time [5, 6]. The ballistic photons arriving first produce an unblurred but noisy image. Progressively, a rapid series of images are taken which become less noisy but more blurry. The images are then combined to produce a final image, see Fig. 1 for visualization.

Satata *et al.* [5] have shown that using this approach to incorporate diffuse photons in addition to ballistic photons improved the resulting image. This was made possible with a streak camera and a picosecond resolution. Similar approaches with a Single-Photon Avalanche Diode (SPAD) array [7] and a time resolution of 10 to 100ps were presented later [8, 9, 10].

Our key contribution is the development of the deconvolution algorithm for scattering media that accounts for Poisson statistics. The complete information of the captured temporal im-

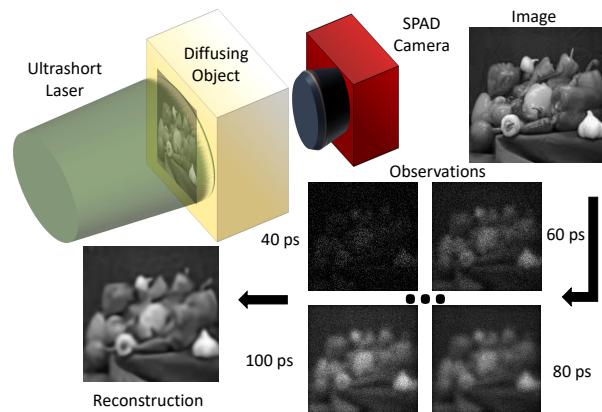


Figure 1: An ultrafast pulsed laser sources illuminates a transmissive object which is placed directly in front of a highly scattering medium. A streak camera is able to resolve the arriving photons in time. Ballistic and scattered photons arrive at different times due since scattered photons travel a longer path. The spatio-temporal imaging system is modeled with a time-dependent point spread function computed from the RTE. Inversion of this model allows reconstruction of a noise free, deconvolved image.

age stack is exploited to compute a deconvolved image. We start by discussing light propagation through scattering media and derive a forward model by analytically solving an approximation of the RTE. Subsequently, we follow the idea of Rond *et al.* [11] for Poisson inversion problems and augment the Plug & Play priors (P&PP) framework [12] with the derived forward model. We leverage the power of a state-of-the-art Deep Learning based denoiser to efficiently regularize the optimization problem. Finally, we validate the deconvolution algorithm with synthetic experiments. We demonstrate that the proposed algorithm performs significantly better than denoising only the ballistic images. We also compare our algorithm to a standard deconvolution technique applied to the blurry, but less noisy time-averaged image.

Computing the Point Spread Function

To combine several progressively blurrier images to produce one higher quality image, we must compute the point spread function of the scattering media for each constituent image. The observed point spread function is changing in time, thus a temporal generalization of the point spread function called the ST-PSF is needed. In this section, light transport theory is used to compute the theoretical ST-PSF for highly scattering media.

Light transport through scattering media is governed by the RTE [13]. The RTE accounts for scattering and absorption events

as well as transport of radiant intensity through scattering media. While very accurate, the full RTE is a six dimensional (3 spatial, 2 angular, 1 temporal) integro-partial differential equation that is challenging to solve both computationally and analytically. In optically thick media, where scattering dominates absorption events, the RTE can be well approximated by a simpler diffusion equation given by

$$\frac{1}{c} \frac{\partial u(\mathbf{r}, t)}{\partial t} = D \nabla^2 u - \mu_a u + S \quad \text{and} \quad u(\mathbf{r}, 0) = f(\mathbf{r}), \quad (1)$$

where c denotes speed of light and $u = u(\mathbf{r}, t)$ is the time dependent intensity at a spatial position $\mathbf{r} = (x, y, z)$, $S = S(\mathbf{r})$ is a source term, μ_a is the absorption coefficient, D is a constant given by

$$D = \frac{1}{3(\mu_a + (1-g)\mu_s)}, \quad (2)$$

with μ_s being the scattering coefficient, and g the scattering anisotropy, see [13] for details on the RTE.

The behavior of a linear (and spatio-temporally) invariant system is characterized by its impulse response. The impulse response of light transmission through scattering media is given by the ST-PSF.

The ST-PSF of this system can be computed by solving Eq. (1) with the illumination coming from an instantaneous point source given by a delta-peak $f(\mathbf{r}) = \delta(\mathbf{r})$ at time $t = 0$ and $S = 0$. Fourier transforming Eq. (1) yields

$$\frac{1}{c} \frac{\partial \hat{u}}{\partial t} = -D|\boldsymbol{\omega}|^2 \hat{u} - \mu_a \hat{u}, \quad (3)$$

where \hat{u} denotes the Fourier coefficient for wave vector $\boldsymbol{\omega}$. This integrates to

$$\hat{u} = e^{-D(|\boldsymbol{\omega}|^2 - \mu_a)ct}. \quad (4)$$

Using the Fourier inversion formula yields

$$u = \frac{c}{(4\pi cDt)^{3/2}} \exp\left(-\frac{|\mathbf{r}|^2}{4Dct} - \mu_a ct\right). \quad (5)$$

The solution u can be interpreted in terms of a ST-PSF in three dimensional space. To find the ST-PSF we must evaluate this function for each pixel on our sensor. Let us assume that the sensor is a plane located directly behind the scattering medium with thickness z_0 . Our final expression for the ST-PSF, denoted as h , will be given by:

$$h(x, y, t; z_0) = \frac{c}{(4\pi cDt)^{3/2}} \exp\left(-\frac{x^2 + y^2 + z_0^2}{4Dct} - \mu_a ct\right). \quad (6)$$

An example for a ST-PSF with typical parameters [14] for human tissue is visualized in Fig. 2. At first glance, highly scattered photons do not seem to carry any meaningful information. However, there is a much higher number of photons available when compared to the ballistic photons. It is not so far-fetched that the higher SNR in later time bins can be exploited in a meaningful way. One gets measurements of highly scattered photons for free since they are captured by the streak camera, but usually discarded.

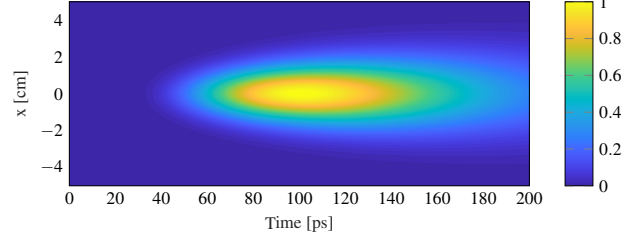


Figure 2: The energy and width of the ST-PSF grow in time. Initial time slices have little blurring, but low energy. Later time slices have more energy, but significant blurring. The ST-PSF was created with $\mu_s = 5 \text{ cm}^{-1}$, $\mu_a = 1 \text{ cm}^{-1}$, $g = 0.99$ and a scattering volume with depth 3 cm. These are typical parameters for human skin [15]. The displayed image is shown for visualization purposes only and the intensity is in arbitrary units.

Reconstruction Algorithm

In this section we first discuss a model of the image formation process under the diffusion approximation for scattering media. We then propose a novel method to recover an undistorted image from the observation by maximizing a likelihood function assuming a Poisson noise model. Due to the high noise in the images of the ballistic photons, regularization terms are needed. For image reconstruction, we leverage the P&PP [12] framework. This allows us to include a state-of-the-art denoiser, implemented as a neural network, for an efficient optimization of the problem.

Forward Model

A complete model includes the ST-PSF diffusion of light propagating from a source, through a scattering media, to an object and finally to the sensor. In this work we ignore the space-time blurring from the source to object, and only model blur from object to detector.

We assume the imaging scenario visualized in Fig. 1. An ultra fast laser illuminates a 2-dimensional object $o(x, y)$ which is placed directly in front of a homogeneously scattering media of depth z_0 . After travelling through the media, the light is subsequently captured by a camera with a high temporal resolution. The noise free image $I(x, y, t)$ expected at time t is modeled as a convolution with the ST-PSF $h(x, y, t; z_0)$ as

$$I(x, y, t) = \int o(x - x', y - y') \cdot h(x', y', t; z_0) dx' dy', \quad (7)$$

Let $\mathbf{o} \in \mathbb{R}^N$ be the one dimensional discretization of the 2-dimensional object o written as a column vector. Let $\mathbf{m}^k = [m_j^k] \in \mathbb{R}^N$ be the discretized image observed at time k , and m_j^k the measured photon count in pixel j at time k . In this work we assume that the observed images $\mathbf{m}^k, k = 1, \dots, K$ are corrupted by Poisson noise which produces the following observation model:

$$P(\mathbf{m}^k | \mathbf{o}) \propto \prod_{j=1}^N \left(\mathbf{e}_j^T \mathbf{H}^k \mathbf{o} \right)^{m_j^k} e^{-\mathbf{e}_j^T \mathbf{H}^k \mathbf{o}}, \quad (8)$$

where $\mathbf{H}^k \in \mathbb{R}^{N \times N}$ is the block-circulant convolution matrix associated with the convolution kernel in Eq. (6) at time $t = k$, and $\mathbf{e}_j \in \mathbb{R}^N$ is the j^{th} vector of the canonical basis of \mathbb{R}^N .

Assuming that the observations are independently acquired,

the likelihood of our model is given as

$$P(\mathbf{m}^1, \dots, \mathbf{m}^K | \mathbf{o}) \propto \prod_{k=1}^K P(\mathbf{m}^k | \mathbf{o}) . \quad (9)$$

In order to reconstruct the object \mathbf{o} we need to calculate the negative log-likelihood which can be easily obtained from Eq. (8) as

$$L(\mathbf{o}) = \text{const.} + \sum_{k=1}^K \sum_{j=1}^N \mathbf{e}_j^T \mathbf{H}^k \mathbf{o} - m_j^k \log(\mathbf{e}_j^T \mathbf{H}^k \mathbf{o}) , \quad (10)$$

and its gradient, which is given by

$$\frac{\partial}{\partial \mathbf{o}} L(\mathbf{o}) = \sum_{k=1}^K (\mathbf{H}^k)^T \left\{ \mathbb{1} - \mathbf{m}^k ./ (\mathbf{H}^k \mathbf{o}) \right\} , \quad (11)$$

where $\mathbb{1} \in \mathbb{R}^N$ is a vector with all its components equal to 1, and $./$ represents element-wise division.

Plug-and-Play Prior

Venkatakrishnan *et al.* proposed P&PP [12], a flexible framework that accommodates a wide-variety of state-of-the-art priors, such as denoising models, in forward model based image reconstruction algorithms. Rond *et al.* [11] adapted the P&PP framework for imaging problems corrupted by Poisson noise. One particularity of P&PP is that even though the observed measurements may follow Poisson statistics, a Gaussian denoiser can still be employed.

The goal of the P&PP framework is to solve a regularized optimization problem, in our case:

$$\hat{\mathbf{o}} = \arg \min_{\mathbf{o}} L(\mathbf{o}) + \beta \varphi(\mathbf{o}) , \quad (12)$$

where β denotes the regularization parameter for the regularization function φ , which does not need to be explicitly known.

P&PP transforms the problem in Eq. (12) into the following constrained optimization problem

$$\hat{\mathbf{o}}, \hat{\mathbf{v}} = \arg \min_{\mathbf{o}, \mathbf{v}} L(\mathbf{o}) + \beta \varphi(\mathbf{v}) \quad \text{s.t.} \quad \mathbf{o} = \mathbf{v} , \quad (13)$$

which is solved using the Alternating Direction Method of Multipliers (ADMM) algorithm [16]. We begin by constructing an augmented Lagrangian L_λ with parameter λ of the form

$$L_\lambda(\mathbf{o}, \mathbf{v}, \mathbf{u}) = L(\mathbf{o}) + \beta \varphi(\mathbf{v}) + \frac{\lambda}{2} \|\mathbf{o} - \mathbf{v} + \mathbf{u}\|_2^2 - \frac{\lambda}{2} \|\mathbf{u}\|_2^2 \quad (14)$$

which would be classically minimized iteratively by cycling through the following three steps

$$\mathbf{o}_{i+1} = \arg \min_{\mathbf{o}} L(\mathbf{o}) + \frac{\lambda}{2} \|\mathbf{o} - \mathbf{v}_i + \mathbf{u}_i\|_2^2 \quad (15a)$$

$$\mathbf{v}_{i+1} = \arg \min_{\mathbf{v}} \frac{\lambda}{2} \|\mathbf{o}_{i+1} - \mathbf{v} + \mathbf{u}_i\|_2^2 + \beta \varphi(\mathbf{v}) , \quad (15b)$$

$$\mathbf{u}_{i+1} = \mathbf{u}_i + (\mathbf{o}_{i+1} - \mathbf{v}_{i+1}) . \quad (15c)$$

The second step has the form of a Gaussian denoiser and can be replaced with an arbitrary Gaussian denoiser with noise variance $\sigma^2 = \frac{\beta}{\lambda}$ and prior $\varphi(\mathbf{v})$ [11, 17]. This finding is particularly interesting because the prior no longer needs to be specified.

Algorithm 1 Transient image deconvolution

Input: Transient images \mathbf{m}^k , forward model \mathbf{H}^k , FFDNet

Initialization: $i = 0; \mathbf{u}_0 = \mathbf{0}; \mathbf{o}_0 = \mathbf{0}; \mathbf{v}_0 = \mathbf{0}, \lambda_0 = 1.$

while !stopping criteria **do**

$$\mathbf{o}_{i+1} = \arg \min_{\mathbf{o}} L(\mathbf{o}) + \frac{\lambda_i}{2} \|\mathbf{o} - \mathbf{v}_i + \mathbf{u}_i\|_2^2$$

$$\mathbf{v}_{i+1} = \text{FFDNet}_\sigma(\mathbf{o}_{i+1} + \mathbf{u}_i) \quad \text{with} \quad \sigma^2 = \frac{\beta}{\lambda_i}$$

$$\mathbf{u}_{i+1} = \mathbf{u}_i + (\mathbf{o}_{i+1} - \mathbf{v}_{i+1})$$

$$\lambda_{i+1} = \lambda_i \cdot \lambda_{step}$$

Output: Reconstructed image \mathbf{o}_i

Zhang *et al.* [17] provide a comprehensive comparison of the influence of the denoiser on typical image restoration problems for a framework very similar to the discussed one. They show that a deep-learning based denoiser performs as well or better while having much lower computational than most state-of-the-art denoisers. For the Poisson inversion problems Rond *et al.* [11] chose the dictionary learning based denoiser proposed in [18]. In this paper, we use FFDNet, a deep learning based denoiser proposed by Zhang *et al.* [19] based on a convolutional neural network due to the findings of [17]. FFDNet has shown excellent denoising results while keeping the computation time short due to an efficient GPU implementation. FFDNet is available for download with the open source Matlab toolbox MatConvNet [20].

Following [16], parameter λ is increased at each iteration by successively multiplying it by a scalar $\lambda_{step} > 1$. The parameter λ_{step} allows us to scale our regularization parameter and denoising parameter to adapt to our less noisy image. In all our experiments we have chosen an initial $\lambda_0 = 1$, $\lambda_{step} = 1.1$, and $\beta = 0.25$. However, the reconstruction depends highly on these parameters and varying them might significantly improve or worsen the reconstruction quality.

The update of image \mathbf{o}_i contains the likelihood function and corresponds to the deconvolution problem. Its optimization is convex and can be efficiently solved with the Limited-memory Broyden-Fletcher-Goldfarb-Shanno algorithm provided in the Matlab framework *minFunc*, written by Schmidt [21]. Equations (10) and (11) are used as input. For values close to 0 the logarithm produces significant numerical errors, thus we replace the pointwise logarithm with the following surrogate function in Eq. (10) [11]

$$\kappa(\xi) = \begin{cases} \log(\xi), & \text{if } \xi > \varepsilon \\ a\xi^2 + b\xi + c & \text{otherwise} \end{cases} . \quad (16)$$

Where ε is small and the parameters $a, b,$ and c are chosen so that $\kappa(\xi)$ is continuous and differentiable for all $\xi \geq 0$. In our simulations we set $\varepsilon = 10^{-10}$. The complete restoration process is summarized in Algorithm 1.

Experiments and Results

In our simulation experiments we investigate if information is gained by including the highly scattered, but less noisy photons of later time bins in the reconstruction algorithm instead of denoising only the weakly scattered photons.

For our experiments, we first fix the material parameters. The diffusion anisotropy is set to $g = 0.99$, the absorption and scattering coefficients are set to $\mu_a = 1/\text{cm}$ and $\mu_s = 5/\text{cm}$. We

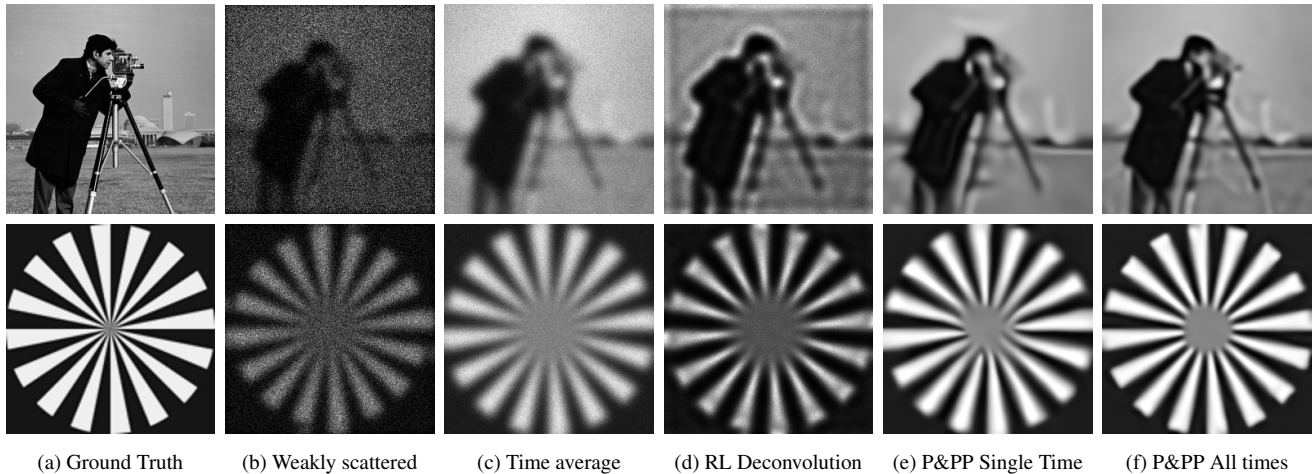


Figure 3: Visual evaluation of the proposed reconstruction algorithm for two simulated images. Weakly scattered images are subject to heavy noise (b), while later times are heavily blurred with better photon statistics (c). Images (d) show deconvolution with Richardson-Lucy. The proposed algorithm was applied for a single image of an early time at 8 ps, see (e), and for a reconstruction considering the full temporal image stack, see Images (f). Reconstruction with the temporally resolved images shows the best reconstruction result.

choose a field of view of 50 cm and assume a homogeneously scattering volume with a depth of 3 cm. The total exposure time is set to $t_{End} = 120$ ps. For the chosen configuration, 120 ps coincides roughly with the time of maximal photon arrival in the ST-PSF, see Fig. 2. For times after the maximal photon arrival, the captured images are not only blurrier, but also become noisier again since fewer photons arrive. We further fix the light budget emitted by the light source, by normalizing the discretized version of the ST-PSF to carry $N_{ST-PSF} = 450$ photons in total. Thus, depending on the chosen time-sampling interval, each time bin exhibits different noise statistics. We choose a sampling time of $\Delta t = 4$ ps. For times until 40 ps the ST-PSF's total energy is less than a single photon, so we discard the first 10 images since they provide no information. Eventually, we observe 20 images where the maximum photon counts per pixel vary from a very few pixels for early times up to about 30 photons for later time slices. Different application domains can be modeled by scaling the distances and modifying the scattering parameters.

To evaluate the proposed algorithm, we first compare the reconstruction results of the complete temporal image stack against a standard Richardson-Lucy (RL) deconvolution [22]. For the comparison, the RL is applied to each image in the stack as well as to the time-averaged signal which has better photon statistics but is more blurred. We also apply our proposed algorithm to all time-slices individually to investigate if the deconvolution of the single image provides better results. Reconstruction results are shown in Fig. 3 and are quantitatively evaluated for the cameraman-example in Fig. 4. RL deconvolution of individual images does not perform well since each image is very noisy, see Fig. 1 and RL for time-averaged signal performs slightly better but it is still of poor quality. Deconvolution of single time-slices with the proposed P&PP-framework achieves much better reconstruction results, however high frequencies still cannot be resolved. P&PP reconstruction with the full temporal stack provides a significantly improved reconstruction. Much higher frequencies are reconstructed while maintaining a denoised version of the imaged scene.

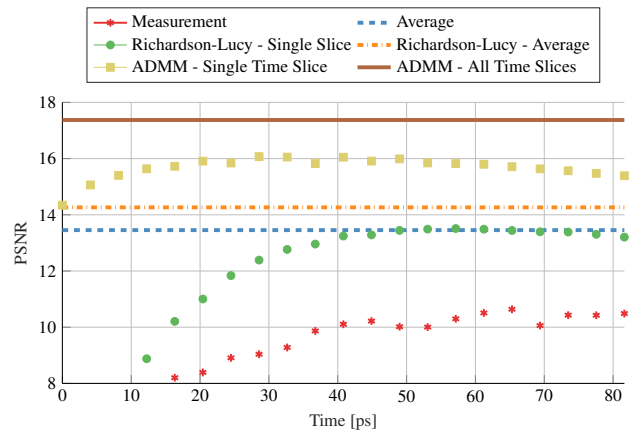


Figure 4: The figure shows the PSNR for raw measurements, Richardson-Lucy deconvolution and the proposed ADMM framework. Points represent reconstruction of only one time slice, lines mean that photons from all time slices are used.

Conclusion and Outlook

In this paper we have proposed a novel deconvolution approach for transient imaging through highly scattering media. The scattering media is described by the diffusion assumption of the RTE, whose solution provides the ST-PSF used for our forward model. We then propose an adaption of P&PP for Poisson inverse problems to deconvolve the temporal stack of images. The algorithm is able to significantly improve the image quality using time-resolved data compared to the time averaged signal and deconvolution of images containing only weakly scattered photons.

For the next steps we intend to evaluate the proposed algorithm with real experiments. We will further investigate how the reconstruction algorithms can be extended to cope with arbitrary three dimensional objects placed in scattering media. Furthermore, since the diffusion approximation is valid only for highly scattering media we will investigate how this constraint can be relaxed to work with low-scattering images.

A major drawback of the ADMM framework is its strong dependence on the regularization parameters β , λ_0 and λ_{step} . Ruiz *et al.* [23] proposed to estimate the unknown optimal regularization parameters in the ADMM through a Bayesian framework. Further research will be devoted to apply similar approaches to engineer an automatic framework with little to no manual user input.

References

- [1] M. G. Tanner, T. R. Choudhary, T. H. Craven, B. Mills, M. Bradley, R. K. Henderson, K. Dhaliwal, and R. R. Thomson, "Ballistic and snake photon imaging for locating optical endomicroscopy fibres," *Biomedical optics express*, vol. 8, no. 9, pp. 4077–4095, 2017.
- [2] N. Hautière, R. Labayrade, C. Boussard, J. Tarel, and D. Aubert, "Perception through scattering media for autonomous vehicles," *Autonomous Robots Research Advances*, vol. 8, pp. 223–267, 2008.
- [3] L. Wang, P. P. Ho, C. Liu, G. Zhang, and R. R. Alfano, "Ballistic 2-d imaging through scattering walls using an ultrafast optical kerr gate," *Science*, vol. 253, no. 5021, pp. 769–771, 1991.
- [4] K. M. Yoo, F. Liu, and R. R. Alfano, "Imaging through a scattering wall using absorption," *Optics Letters*, vol. 16, no. 14, pp. 1068, 1991.
- [5] G. Satat, B. Heshmat, D. Raviv, and R. Raskar, "All photons imaging through volumetric scattering," *Scientific Reports*, vol. 6, no. 1, 2016.
- [6] A. Lyons, A. Boccolini, F. Tonolini, A. Repetti, Z. Chen, J. Leach, R. Henderson, Y. Wiaux, and D. Faccio, "Diffuse time-of-flight imaging with a single-photon camera," in *Imaging and Applied Optics 2018*. 2018, OSA.
- [7] G. Gariépy, N. Krstajić, R. Henderson, C. Li, R. R. Thomson, G. S. Buller, B. Heshmat, R. Raskar, J. Leach, and D. Faccio, "Single-photon sensitive light-in-flight imaging," *Nature Communications*, vol. 6, no. 1, 2015.
- [8] A. Boccolini, F. Tonolini, J. Leach, R. Henderson, and D. Faccio, "Imaging inside highly diffusive media with a space and time-resolving single-photon sensor," in *Imaging Systems and Applications*. Optical Society of America, 2017.
- [9] A. Lyons, A. Boccolini, F. Tonolini, A. Repetti, Z. Chen, R. Henderson, Y. Wiaux, and D. Faccio, "Computational time-of-flight diffuse optical tomography," *arXiv preprint arXiv:1808.01135*, 2018.
- [10] G. Satat, M. Tancik, and R. Raskar, "Imaging through volumetric scattering with a single photon sensitive camera," in *Mathematics in Imaging*. Optical Society of America, 2018.
- [11] A. Rond, R. Giryes, and M. Elad, "Poisson inverse problems by the plug-and-play scheme," *Journal of Visual Communication and Image Representation*, vol. 41, pp. 96–108, 2016.
- [12] S. V. Venkatakrisnan, C. A. Bouman, and B. Wohlberg, "Plug-and-play priors for model based reconstruction," in *2013 IEEE Global Conference on Signal and Information Processing*. 2013, IEEE.
- [13] A. Ishimaru, *Wave propagation and scattering in random media*, IEEE Press, 2005.
- [14] S. L. Jacques, "Optical properties of biological tissues: a review," *Physics in Medicine and Biology*, vol. 58, no. 11, 2013.
- [15] J. L. Sandell and T. C. Zhu, "A review of in-vivo optical properties of human tissues and its impact on PDT," *Journal of Biophotonics*, vol. 4, no. 11-12, pp. 773–787, 2011.
- [16] S. Boyd, "Distributed optimization and statistical learning via the alternating direction method of multipliers," *Foundations and Trends in Machine Learning*, vol. 3, no. 1, pp. 1–122, 2010.
- [17] K. Zhang, W. Zuo, S. Gu, and L. Zhang, "Learning deep CNN denoiser prior for image restoration," in *2017 IEEE Conference on Computer Vision and Pattern Recognition (CVPR)*, 2017.
- [18] J. Sulam, B. Ophir, and M. Elad, "Image denoising through multi-scale learnt dictionaries," in *2014 IEEE International Conference on Image Processing (ICIP)*, 2014.
- [19] K. Zhang, W. Zuo, and L. Zhang, "FFDNet: Toward a fast and flexible solution for CNN-based image denoising," *IEEE Transactions on Image Processing*, vol. 27, no. 9, pp. 4608–4622, 2018.
- [20] A. Vedaldi and K. Lenc, "Matconvnet – convolutional neural networks for matlab," in *Proceeding of the ACM Int. Conf. on Multimedia*, 2015.
- [21] M. Schmidt, "minfunc: unconstrained differentiable multivariate optimization in matlab," *Software available at <http://www.cs.ubc.ca/~schmidtm/Software/minFunc.htm>*, 2005.
- [22] D. S. C. Biggs and M. Andrews, "Acceleration of iterative image restoration algorithms," *Applied optics*, vol. 36, no. 8, pp. 1766–1775, 1997.
- [23] P. Ruiz, R. Molina, and A. K. Katsaggelos, "Joint data filtering and labeling using gaussian processes and alternating direction method of multipliers," *IEEE Transactions on Image Processing*, vol. 25, no. 7, pp. 3059–3072, 2016.

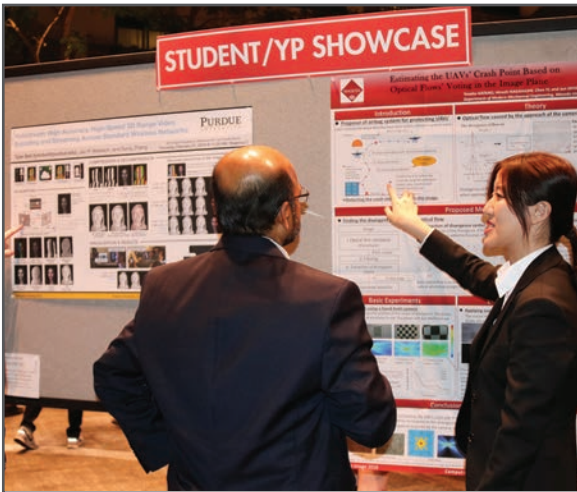
JOIN US AT THE NEXT EI!

IS&T International Symposium on

Electronic Imaging

SCIENCE AND TECHNOLOGY

Imaging across applications . . . Where industry and academia meet!



- **SHORT COURSES • EXHIBITS • DEMONSTRATION SESSION • PLENARY TALKS •**
- **INTERACTIVE PAPER SESSION • SPECIAL EVENTS • TECHNICAL SESSIONS •**

www.electronicimaging.org

